ISSN 0021-8944, Journal of Applied Mechanics and Technical Physics, 2021, Vol. 62, No. 4, pp. 654–662. © Pleiades Publishing, Ltd., 2021.
Russian Text © G.S. Yan'kova, A.A. Cherevko, A.K. Khe, O.B. Bogomyakova, A.A. Tulupov.

MATHEMATICAL MODELING OF NORMAL-PRESSURE HYDROCEPHALUS AT DIFFERENT LEVELS OF THE BRAIN GEOMETRY DETALIZATION

G. S. Yan'kova[a,b,*], A. A. Cherevko[a,b], A. K. Khe[a,b], O. B. Bogomyakova[c], and A. A. Tulupov[b,c]

UDC 51-76; 519.63

Abstract: This paper describes the use of a multiphase model of poroelasticity meant for the brain substance and based on medical data to study the displacement of a ventricle wall in the brain and the value of pressure on it. The dependence of displacement and pressure on the parameters of the model in normal-pressure hydrocephalus is studied. It is shown for different levels of the brain geometry detalization that the simplified geometry of the brain allows one to estimate critical pressures and displacements in the case of more complex geometry.

Keywords: poroelasticity, finite element method, normal-pressure hydrocephalus, cerebrospinal fluid, magnetic resonance imaging.

DOI: 10.1134/S0021894421040155

INTRODUCTION

A number of neurological diseases are associated with disorders of the cerebrospinal fluid (CSF) circulation. One of these pathologies is hydrocephalus, characterized by pathological enlargement of the ventricles of the brain due to excessive accumulation of CSF. One of the forms of hydrocephalus is normal-pressure hydrocephalus (NPH) in which intracranial pressure slightly differs from a normal value. This form of hydrocephalus, characterized by gait disorder, urinary incontinence, and dementia [1, 2], is difficult to diagnose, so it is difficult to make surgery plans. The most common treatment for NPH is bypass surgery, which removes excess CSF from the cranial cavity. However, this method of treatment can help one achieve a positive result only in 50–60% of cases [3]. Moreover, according to [3, 4], patients who are diagnosed and prescribed treatment at an early stage of NPH respond better to treatment.

Magnetic resonance imaging (MRI) is one of the main methods of in vivo study of the CSF system of humans. It is used for noninvasive quantitative and qualitative estimation of the dynamics of CSF circulation in both normal and pathological conditions. This research method can be used to visualize the CSF flow, quantify its velocity, and analyze the structural state of the brain substance [5]. Thus, MRI is currently the most effective method for diagnosing NPH and monitoring its development. Also of great importance is the observation of intracranial pressure, which can only be measured invasively.

However, the current state of medicine does not allow for a long-term and continuous reception of data on processes in the brain. Therefore, NPH has not been sufficiently studied: its origin is not entirely clear, and

[a]Lavrent'ev Institute of Hydrodynamics, Siberian Branch, Russian Academy of Sciences, Novosibirsk, 630090 Russia. [b]Novosibirsk State University, Novosibirsk, 630090 Russia. [c]International Tomography Center, Siberian Branch, Russian Academy of Sciences, Novosibirsk, 630090 Russia; *galinayankova2703@gmail.com, cherevko@mail.ru, alekhe@hydro.nsc.ru, bogom_o@tomo.nsc.ru, taa@tomo.nsc.ru. Translated from Prikladnaya Mekhanika i Tekhnicheskaya Fizika, Vol. 62, No. 4, pp. 148–157, July–August, 2021. Original article submitted April 30, 2021; revision submitted May 11, 2021; accepted for publication May 31, 2021.

*Corresponding author.

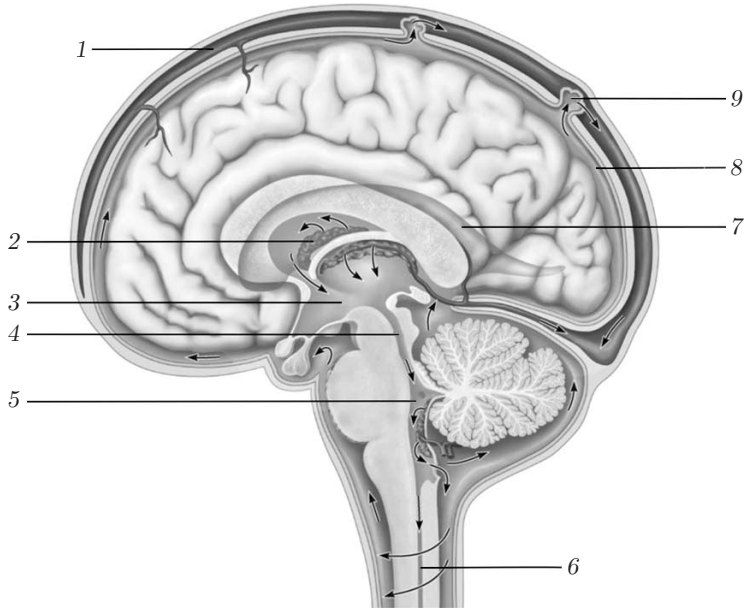

Fig. 1. CSF circulation diagram: (*1*) superior sagittal sinus, (*2*) vascular plexus, (*3*) third ventricle, (*4*) Sylvian aqueduct, (*5*) fourth ventricle, (*6*) central spinal canal, (*7*) right lateral ventricle, (*8*) subarachnoid space, and (*9*) arachnoid granulation.

it is difficult to predict its course. As a result, various hypotheses have been put forward about the causes and pathophysiology of NPH. As these hypotheses have not yet led to a complete understanding of the causes and mechanisms of the formation and development of hydrocephalus, it is advisable to use mathematical modeling to study this pathological condition. Constructing an adequate mathematical model requires that the nature of the flow and interaction of CSF in the brain is investigated.

The extracellular fluids of the brain are blood, CSF, and intercellular fluid. CSF is a transparent liquid, whose density and viscosity are close to those of water. It is known that CSF is formed by filtration of capillary blood plasma through a vascular plexus epithelium in all four ventricles, which is a system of cavities located in the center of the brain. CSF flows from the ventricles into the subarachnoid space of the spinal cord and brain. The bulk of the CSF is drained into a system of venous sinuses of the dura mater (Fig. 1). Also, CSF is absorbed along blood vessels (a so-called glymphatic system) and along meningeal lymphatic vessels into an extracranial lymphatic system. It was shown in [6] that CSF seeps into the brain parenchyma and mixes with the intercellular fluid, thereby clearing the brain from the waste products of metabolites and cells. Moreover, CSF acts as a hydraulic shock absorber for the brain and ensures the delivery of nutrients.

Intracranial hemoliquorodynamics plays a major role in the healthy operation of the brain as disturbances in the dynamics of the fluid medium of the brain can cause multiple complications. It is believed that it is the violation of hemoliquorodynamics that is the cause of NPH. Therefore, obtaining data on pathological processes and providing better treatment can only be possible with understanding of the CSF hydrodynamics and the CSF relationship with blood flow and intracranial pressure.

1. MATHEMATICAL MODELING

Mathematical models describing intracranial dynamics in the normal condition and with a disease can be classified as follows: compartment models dependent only on time ($(P{-}V)$ models (pressure — volume)) [7–9], models that consider the brain parenchyma as a rheologically complex deformable continuous medium [10–14], models using computational fluid dynamics (CFD) [15–18], and mechanical models that interpret the brain parenchyma as a porous material saturated with fluid and deforming in accordance with the interaction of tissue and pore fluids [19–22].

Compartment models make it possible to describe the physiology and pathophysiology of diseases, but they are often difficult to implement, which limits their application in a clinical setting. CFD modeling allows determining the pressure and velocity fields of the brain fluids for patient-specific geometry. However, the drawback of most of the existing models is that they do not describe an interaction among the circulatory network of the brain, parenchyma, and CSF. This disadvantage can be eliminated by refining the existing mechanical models based on the theory of poroelasticity. In this work, a model similar to that proposed in [21] is used.

1.1. Mathematical Model

A multifluid poroelastic filtration model is used. It is assumed that the brain parenchyma is modeled by a porous matrix, and there are liquid phases located at each point of the pore space and communicating with each other: arterial blood (values with subscript a), capillary blood (values with subscript c), venous blood (values with subscript v), and CSF (values with subscript e). Each liquid phase is characterized by its own pressure. The exchange of liquids between phases is shown in Fig. 2. This model takes into account the distribution and mutual influence of pressures in the phases under consideration, as well as the influence of these pressures on the displacement of the brain substance.

Mathematical modeling is performed in a two-dimensional approximation. The geometric model is a sagittal section of the brain [17] obtained using MRI (Fig. 3). The modeling of mechanical processes occurring in the brain using two-dimensional sections is widespread [10, 14, 17, 23]. The choice of a sagittal section is due to the fact that it is located in the symmetry plane, which is why possible differences between two- and three-dimensional deformations are minimized (this section remains generally flat in the case of three-dimensional deformations) and which is why it passes through the anatomical structures under study.

An inner boundary denoted as Γ_V represents a boundary between cerebral ventricles, and an outer boundary denoted as Γ_S corresponds to the boundary of the skull. According to clinical studies, the properties of white and gray matter differ. However, there are no experimental data to quantify these differences at the current time, so the brain parenchyma Ω is modeled as a homogeneous material [21, 24, 25].

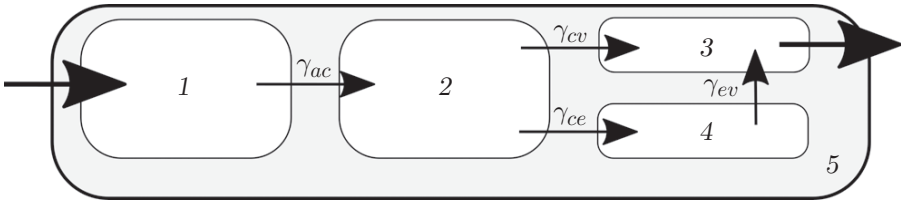

Fig. 2. Blood and CSF transfer in the parenchyma of the brain: (*1*) arterial territory, (*2*) capillary territory, (*3*) venous territory, (*4*) CSF territory, and (*5*) parenchyma.

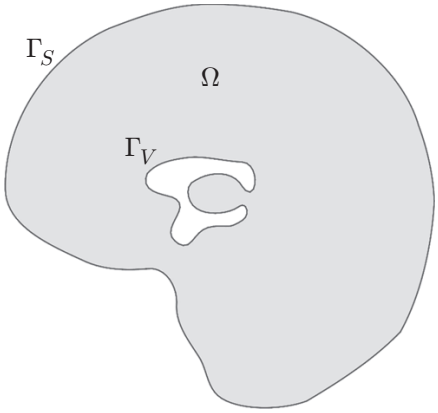

Fig. 3. MRI-based geometry of the parenchyma Ω.

An equilibrium equation for the brain substance has the form [26]

$$\mu\Delta\boldsymbol{u} + (\mu+\lambda)\nabla(\operatorname{div}\boldsymbol{u}) - (\alpha_a\nabla p_a + \alpha_c\nabla p_c + \alpha_e\nabla p_e + \alpha_v\nabla p_v) = 0. \tag{1}$$

The law of conservation of mass and Darcy's law for pore fluids are used to obtain the following equations

$$-(k_a/\mu_a)\,\Delta p_a + |\dot{s}_{ac}| = 0; \tag{2}$$

$$-(k_c/\mu_c)\,\Delta p_c - |\dot{s}_{ac}| + |\dot{s}_{ce}| + |\dot{s}_{cv}| = 0; \tag{3}$$

$$-(k_e/\mu_e)\,\Delta p_e - |\dot{s}_{ce}| + |\dot{s}_{ev}| = 0; \tag{4}$$

$$-(k_v/\mu_v)\,\Delta p_v - |\dot{s}_{cv}| - |\dot{s}_{ev}| = 0. \tag{5}$$

In Eqs. (1)–(5), $\boldsymbol{u}$ denotes the displacement of the brain substance, λ and μ are the elastic moduli, p_i is the pressure of the corresponding pore fluid, α_i and k_i are the Biot and permeability coefficients, μ_i is the viscosity of the pore fluids, and $i = a, c, v, e$. It is assumed that the unidirectional fluid transfer from network x to network y is due to a hydrostatic pressure gradient:

$$\dot{s}_{yx} = -\gamma_{yx}[p_x - p_y]. \tag{6}$$

Here γ_{yx} denotes the coefficient setting the transfer of pore fluids between different territories. System (1)–(5) is supplemented with boundary conditions for the displacement and four pore pressures. On the boundary between the ventricles of the brain Γ_V, the following conditions are set.

1. Stresses are assumed to be continuous:

$$2\mu\varepsilon(\boldsymbol{u})\cdot\boldsymbol{n} + \lambda\epsilon(\boldsymbol{u})\boldsymbol{n} = \sum_{i=a,c,e,v}(\alpha_i - 1)p_i\boldsymbol{n} \tag{7}$$

($\varepsilon(\boldsymbol{u})$ denotes the strain tensor, $\epsilon(\boldsymbol{u}) = \operatorname{tr}\varepsilon(\boldsymbol{u}) = \varepsilon(\boldsymbol{u})_{ii} = \operatorname{div}\boldsymbol{u}$, and $\boldsymbol{n}$ is the outer unit normal vector).

2. No flow for arterial and venous networks:

$$\nabla p_a\boldsymbol{n} = \nabla p_v\boldsymbol{n} = 0. \tag{8}$$

3. CSF is secreted at a constant rate Q_p in the ventricles of the brain. Under the condition of conservation of the fluid mass, the following parameters are accounted for in the ventricular system: the volume of the CSF produced by the vascular plexuses, the volume of CSF that seeps through the wall of the ventricles, the outflow of the cerebrospinal fluid through the Sylvian aqueduct.

$$Q_p = \frac{\pi d^4}{128\mu L}\,(p_e\Big|_{\Gamma_V} - p_e\Big|_{\Gamma_S}) - \oint\limits_{\Gamma_V}\Big(-\frac{k_e}{\mu_e}\,\nabla p_e\Big)\cdot\boldsymbol{n}\,dS \tag{9}$$

(d and L denotes the diameter and length of the Sylvian aqueduct).

4. The formation of CSF from blood reduces pressure in the capillary network:

$$\varkappa_{cv}\nabla p_c\boldsymbol{n} = Q_p. \tag{10}$$

Here $\varkappa_{cv}$ is the resistance of the flow penetrating from the capillary network into the ventricles through the vascular plexus.

The following assumptions are made on the skull boundary Γ_S.

1. As this study deals with an adult person's brain, the skull is considered to be rigid. Thus, the displacements of the skull boundary are equal to zero:

$$\boldsymbol{u} = 0. \tag{11}$$

2. There is no capillary flow on the skull boundary:

$$\nabla p_c\boldsymbol{n} = 0. \tag{12}$$

3. The values of arterial and venous pressures are set:

$$p_a = p_{art}, \qquad p_v = p_{ven}. \tag{13}$$

4. CSF absorption into the venous network increases the pressure:

$$p_e = p_v + \mu_e R Q_0 \tag{14}$$

(R is the resistance caused by the presence of arachnoid granulations, Q_0 is the CSF outflow into the venous network, and μ_e is the CSF viscosity).

According to [27, 28], the quantities characterizing the pore fluids and the porous matrix have the following values: $E = 584$ Pa [29], $\nu = 0.35$, $k_{a,c,v} = 10^{-10}$ m^2, $k_e = 1.4 \cdot 10^{-14}$ m^2, $\mu_{a,c,v} = 2.67 \cdot 10^{-3}$ (N$\cdot$s)/m^2, $\mu_e = 8.9 \cdot 10^{-4}$ (N$\cdot$s)/m^2, $p_{art} = 8000$ Pa, $p_{ven} = 650$ Pa, $Q_p = Q_0 = 5.8 \cdot 10^{-9}$ m^3/s, $d = 0.004$ m, $L = 0.07$ m, $R = 8.5 \cdot 10^{13}$ m^{-3}, $\varkappa_{cv} = 6 \cdot 10^{-4}$ (m$^5 \cdot$s)/kg [22, 28], $\alpha_{a,e,c,v} = 0.99$.

With account for Young's modulus E and Poisson's ratio ν, the elastic moduli λ and μ calculated using the known expressions

$$\lambda = \frac{\nu E}{(1+\nu)(1-2\nu)}, \qquad \mu = \frac{E}{2(1+\nu)}.$$

1.2. Solution Method

Equations (1)–(5) the boundary conditions (7)–(14) are solved using the finite element method in an open-source software [30]. A weak formation of the problem is obtained by multiplying Eqs. (1)–(5) by the test functions $\bar{\boldsymbol{u}}$, $\bar{p}_a$, $\bar{p}_v$, $\bar{p}_c$, $\bar{p}_e \in H^1(\Omega)$, respectively, and integrating them with respect to domain Ω with account for the boundary conditions

$$\bar{\boldsymbol{u}}\Big|_{\Gamma_S} = 0, \quad \bar{p}_a\Big|_{\Gamma_S} = 0, \quad \bar{p}_v\Big|_{\Gamma_S} = 0, \quad \bar{p}_e|_{\Gamma_S} = 0.$$

The Gauss formula and the boundary conditions (7)–(14) are applied to formulate the problem as follows: we should determine functions $\boldsymbol{u}$, p_a, p_v, p_c, and $p_e \in H^1(\Omega)$, that satisfy the boundary conditions (7)–(14) and the integral relations

$$\int\limits_\Omega \Big(\Big(-\lambda \operatorname{div} \boldsymbol{u} + \sum_{i=a,c,e,v} \alpha_i p_i \Big) \operatorname{div} \bar{\boldsymbol{u}} - 2\mu \varepsilon(\boldsymbol{u}) : \varepsilon(\bar{\boldsymbol{u}}) \Big)\, d\Omega - \int\limits_{\Gamma_V} \Big(\sum_{i=a,c,e,v} p_i \boldsymbol{n} \cdot \bar{\boldsymbol{u}} \Big)\, ds = 0,$$

$$\int\limits_\Omega \Big(\frac{k_a}{\mu_a} \nabla p_a \cdot \nabla \bar{p}_a + |\dot{s}_{ac}| \bar{p}_a \Big)\, d\Omega = 0,$$

$$\int\limits_\Omega \Big(\frac{k_v}{\mu_v} \nabla p_v \cdot \nabla \bar{p}_v + (-|\dot{s}_{cv}| - |\dot{s}_{ev}|) \bar{p}_v \Big)\, d\Omega = 0, \tag{15}$$

$$\int\limits_\Omega \Big(\frac{k_c}{\mu_c} \nabla p_c \cdot \nabla \bar{p}_c + (-|\dot{s}_{ac}| + |\dot{s}_{ce}| + |\dot{s}_{cv}|) \bar{p}_c \Big)\, d\Omega - \int\limits_{\Gamma_V} \frac{k_c}{\mu_c} \frac{Q_p}{\varkappa_{cv}} \bar{p}_c\, ds = 0,$$

$$\int\limits_\Omega \Big(\frac{k_e}{\mu_e} \nabla p_e \cdot \nabla \bar{p}_e + (-|\dot{s}_{ce}| + |\dot{s}_{ev}|) \bar{p}_c \Big)\, d\Omega -$$

$$- \int\limits_{\Gamma_V} \Big(\frac{Q_p}{4\pi (r_1 + u)^2} + \frac{\pi d^4}{4\pi (r_1 + u)^2 \cdot 128 L \mu_e} \left(p_{ven} + \mu_e R Q_0 - p_e \right) \Big) \bar{p}_e\, ds = 0$$

for the arbitrary test functions $\bar{\boldsymbol{u}}$, $\bar{p}_a$, $\bar{p}_v$, $\bar{p}_c$, and $\bar{p}_e$, which satisfy the boundary conditions (15). In the last equation of system (15), the denominator contains the factor $4\pi(r_1 + u)^2$, which corresponds to the spherical approximation of the ventricle surface for the second (integral) term in Eq. (9).

2. RESULTS AND DISCUSSION

This work describes dependences between the displacement of the ventricular wall and capillary pressure on γ_{ac}, γ_{cv}, γ_{ce}, and γ_{ev} for the geometry obtained using MRI scans of a real patient's brain. To obtain these dependences, each parameter γ_{ac}, γ_{cv}, γ_{ce}, γ_{ev} independently acquires values from a 15-element set covering a range of physiologically acceptable parameter values: 0.0001, 0.000 68, 0.0149, 0.1489, 0.8872, 3.8154, 13.1054, 38.2225, 98.5754, 231.567, 507.698, 1063.08, 2181.07, 4531.31, 10 000. Thus, 15^4 variants have been calculated. One of them was calculated for approximately 15 s. The results of these calculations are given below in interpolated form.

2.1. Displacement of the Ventricular Wall

The value of the ventricle displacement is barely affected by $\gamma_{ev} = 10^{-4}$–10^3 D/(N · s) (D is Darcy). In the case of larger values of γ_{ev}, the value of the displacement begins to become larger, increasing at $\gamma_{ev} = 10^4$ D/(N · s) by 3.5 mm. With an increase in γ_{cv} and γ_{ce}, the displacement of the ventricular walls decreases. In the case of small γ_{ce}, larger γ_{ac} correspond to larger displacements of the ventricular wall. For $\gamma_{ce} = 10^2$–10^4 D/(N · s), the nature of the dependence of the displacement of the ventricular wall on γ_{ac} is reversed.

In the domain of small values of γ_{ce}, the ventricle displacements are sufficiently large, which does not correspond to the physiological norm. Small displacements of the ventricles are observed only in the domain of large values of γ_{ce} and at values $\gamma_{ac} > 10^2$ D/(N · s). In this domain, there is a displacement of the ventricular wall, corresponding to the physiological norm: $|\boldsymbol{u}| \leqslant 2$ mm [31].

2.2. Pressure Distribution on the Ventricular Wall

The capillary pressure is barely affected by γ_{ev}. As γ_{cv} and γ_{ce} increase, the capillary pressure on the ventricular wall decreases. Larger values of γ_{ac} correspond to larger values of the capillary pressure.

The values of arterial, venous, and CSF pressures at the ventricle boundary remain approximately constant throughout the parameter range ($p_a = 60.15$ mm Hg, $p_v = 4.88$ mm Hg, and $p_e = 8.18$ mm Hg) and correspond to the physiological norm [32]. The spread in the pressure values does not exceed 0.01 mm Hg.

Based on the computational results, a domain of parameters γ_{ac}, γ_{cv}, γ_{ce}, and γ_{ev} is constructed, corresponding to the physiological norm for the values of the displacement of the ventricular wall and capillary pressure.

2.3. Displacement of the Ventricular Wall and the Behavior of Capillary Pressure in the Cases of Cylindrical and Clinical Geometry

In [33], for the simple geometry of the brain parenchyma, considered in cylindrical approximation, the nature of the displacement of the ventricular walls and the behavior of the capillary pressure at various values of γ_{ac}, γ_{cv}, γ_{ce}, and γ_{ev} are analyzed. Such a simple geometric model allows one to study the behavior of pore pressures and the deformation of the brain substance using ordinary differential equations, thereby having an almost 20-fold increase in the rate of computations. Therefore, the goal is to compare the values of the displacements of the ventricular wall and the capillary pressure obtained for the simplified cylindrical and clinical geometries. As shown by the comparison results, the dependences of the displacement of the ventricular wall and the capillary pressure on γ_{ac}, γ_{cv}, γ_{ce}, and γ_{ev} are in good qualitative agreement. Figure 4 shows the projections of the tolerance range of γ_{ac}, γ_{cv}, γ_{ce}, and γ_{ev} for these two cases onto a three-dimensional space of γ_{ac}, γ_{cv}, and γ_{ce}, which are curved quadrangular tubes.

Figures 4a and 4b show the tolerance ranges of γ_{ac}, γ_{cv}, and γ_{ce}, constructed for cylindrical and clinical geometries, respectively. As shown by the results of comparing these areas in Fig. 4c, the domain corresponding to the cylindrical geometry is nested within the domain corresponding to the clinical geometry. Two pairs of opposite sides of this quadrangle correspond to constraints on the displacement of the ventricular wall and on the capillary pressure on its wall (see Fig. 4d). It can be seen that the pressure constraints mark practically the same region of the space of parameters γ_{ac}, γ_{cv}, and γ_{ce} for both geometries. The sections of the boundaries of the tolerance ranges of parameters γ_{ac}, γ_{cv}, and γ_{ce} for different geometries are approximately parallel to each other. With an increase in γ_{ev}, the relative position of the three-dimensional projections remains the same, but

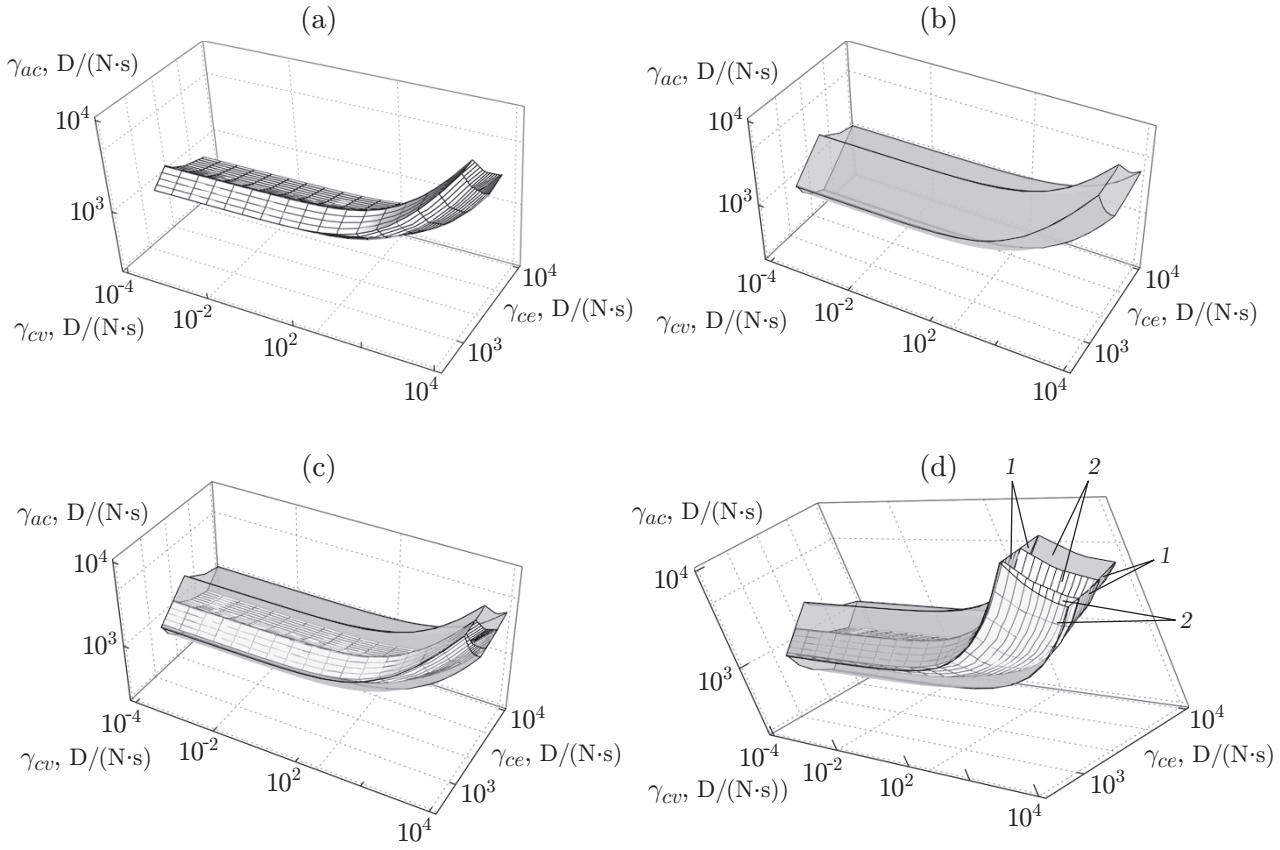

Fig. 4. Domains of the physiological norm in the space of parameters γ_{ac}, γ_{cv}, and γ_{ce} for $\gamma_{ev} = 10^2$ (a–c) and the tolerance range of the capillary pressure (*1*) and of the displacement of the ventricular wall (*2*) (d): (a) for the case of simple geometry [33], (b) for the case of clinical geometry [17], (c) for the cases of simple and clinical geometries.

they are synchronously shifted to the domain of large values of γ_{ce}. This arrangement of the tolerance ranges of γ_{ac}, γ_{cv}, γ_{ce}, and γ_{ev} allow one you to select physiologically acceptable values of γ_{ac}, γ_{cv}, γ_{ce}, and γ_{ev} based on a model with cylindrical geometry, which ensures the physiological validity of these values of γ_{ac}, γ_{cv}, γ_{ce}, and γ_{ev} for a clinical case.

CONCLUSIONS

This work describes the modeling of normal-pressure hydrocephalus in which the intracranial pressure slightly differs from a normal value. The investigation is carried out on the basis of data on the brain geometry obtained with the help of MRI of a real patient's brain. The mathematical basis of the study is a stationary model of multifluid poroelastic filtration. The parenchyma of the brain is modeled using a porous matrix, and communicating liquid phases exist at each point of the pore space: arterial blood, capillary blood, venous blood, and cerebrospinal fluid (CSF). Each liquid phase has its own pressure, and the distribution and mutual influence of these phases are taken into account. The effect of these pressures on the displacement of the brain substance is also taken into account. The equations of poroelastic filtration are supplemented with boundary conditions recorded on the basis of medical data. The resulting boundary-value problem is solved numerically using the finite element method. The displacement of the ventricular wall of the brain and the pressure thereon are considered. The behavior of these quantities is studied for various values of the model parameters in hydrocephalus. For the geometry of the brain with different levels of detail, it is shown how accurately the simplified geometry of the brain allows one to estimate the critical values of pressures and displacements in the case of more complex geometries. In this case, the values

of the critical pressure on the ventricular wall coincide with a high degree of accuracy in the case of simplified and clinical geometry. The displacements of the ventricular wall in the case of simplified geometry make it possible to determine the upper bound of the displacement with high accuracy for the clinical case. This mutual arrangement of the tolerance ranges of the parameters allows one to select their physiologically acceptable values based on a model with simplified geometry, while ensuring the permissibility of these parameters for the clinical case at the same time.

This work was financially supported by the Russian Science Foundation (Grant No. 19-11-00069).

REFERENCES

1. N. R. Graff-Radford and D. T. Jones, "Normal Pressure Hydrocephalus," Lifelong Learning Neurology **25** (1), 165–186 (2019).
2. Z. Wang, Y. Zhang, F. Hu, et al., "Pathogenesis and Pathophysiology of Idiopathic Normal Pressure Hydrocephalus," CNS Neurosci. Therapeut. **26** (12), 1230–1240 (2020).
3. T. Kawaguchi, Y. Hirata, M. Bundo, et al., "Role of Computerized Tomographic Cisternography in Idiopathic Normal Pressure Hydrocephalus," Acta Neurochir. **153** (10), 2041–2048 (2011).
4. O. Algin, "Role of Aqueductal CSF Stroke Volume in Idiopathic Normal-Pressure Hydrocephalus," Amer. J. Neuroradiol. **31** (2), E26–E27 (2010).
5. A. V. Boiko, A. E. Akulov, A. P. Chupakhin, et al., "Measurement of Viscous Flow Velocity and Flow Visualization Using Two Magnetic Resonance Imagers," Prikl. Mekh. Tekh. Fiz. **58** (2), 26–31 (2017) [J. Appl. Mech. Tech. Phys. **58** (2), 209–213 (2017)].
6. G. Yankova, O. Bogomyakova, and A. Tulupov, "The Glymphatic System and Meningeal Lymphatics of the Brain: New Understanding of Brain Clearance," Rev. Neurosci. 1230–1240 (2021).
7. G. Agarwal, B. Berman, and L. Stark, "A Lumped Parameter Model of the Cerebrospinal Fluid System," IEEE Trans. Biomed. Engng., No. 1, 45–53 (1969).
8. T. Takemae, Y. Kosugi, J. Ikebe, et al., "A Simulation Study of Intracranial Pressure Increment Using an Electrical Circuit Model of Cerebral Circulation," IEEE Trans. Biomed. Engng., No. 12, 958–962 (1987).
9. N. Alperin, E. M. Vikingstad, B. Gomez-Anson, and D. N.'Levin, "Hemodynamically Independent Analysis of Cerebrospinal Fluid and Brain Motion Observed with Dynamic Phase Contrast MRI," Magnetic Resonance Medicine **35** (5), 741–754 (1996).
10. P. Agapov, O. M. Belotserkovskii, and I. B. Petrov, "Numerical Simulation of the Consequences of a Mechanical Action on a Human Brain Under a Skull Injury," Comput. Math. Math. Phys. **46** (9), 1629–1638 (2006).
11. J. Van Dommelen, M. Hrapko, and G. Peters, "Constitutive Modelling of Brain Tissue for Prediction of Traumatic Brain Injury," in *Neural Tissue Biomechanics* (Springer, Berlin, 2010).
12. K. Wilkie, C. Drapaca, and S. Sivaloganathan, "Aging Impact on Brain Biomechanics with Applications to Hydrocephalus," Math. Medicine Biology. **29** (2), 145–161 (2012).
13. M. A. Calhoun, S. A. Bentil, E. Elliott, et al., "Beyond Linear Elastic Modulus: Viscoelastic Models for Brain and Brain Mimetic Hydrogels," ACS Biomaterials Sci. Engng. **5** (8), 3964–3973 (2019).
14. I. B. Petrov, "Solution of Deformable Solid Mechanics Dynamical Problems with Use of Mathematical Modeling by Grid-Characteristic Method," in *Continuum Mechanics, Applied Mathematics and Scientific Computing: Godunov's Legacy* (Springer Nature, Cham, 2020).
15. V. Kurtcuoglu, D. Poulikakos, and Y. Ventikos, "Computational Modeling of the Mechanical Behavior of the Cerebrospinal Fluid System," J. Biomech. Engng. **127** (2), 264–269 (2005).
16. S. Gupta, M. Soellinger, P. Boesiger, et al., "Three-Dimensional Computational Modeling of Subject-Specific Cerebrospinal Fluid Flow in the Subarachnoid Space," J. Biomech. Engng. **131** (2), 021010 (2009).
17. N. Masoumi, F. Framanzad, B. Zamanian, et al., "2D Computational Fluid Dynamic Modeling of Human Ventricle System Based on Fluid-Solid Interaction and Pulsatile Flow," Basic Clinic. Neurosci. **4** (1), 64–75 (2013).
18. J. Apura, J. Tiago, A. Bugalho de Moura, et al., "The Effect of Ventricular Volume Increase in the Amplitude of Intracranial Pressure," Comput. Methods Biomech. Biomed. Engng. **22** (9), 1–12 (2019).
19. A. Smillie, I. Sobey, and Z. Molnar, "A Hydroelastic Model of Hydrocephalus," J. Fluid Mech. **539**, 417–443 (2005).
20. B. Wirth, *A Mathematical Model for Hydrocephalus: MS Thesis* (Trinity, 2005).

21. B. Tully and Y. Ventikos, "Cerebral Water Transport Using Multiple-Network Poroelastic Theory: Application to Normal Pressure Hydrocephalus," J. Fluid Mech. **667**, 188–215 (2011).
22. J. Vardakis, B. Tully, and Y. Ventikos, "Multicompartmental Poroelasticity as a Platform for the Integrative Modelling of Water Transport in the Brain," in *Computer Models in Biomechanics* (Springer Sci. Business Media, Dordrecht, 2013).
23. S. Cheng, E. Jacobson, and L. Bilston, "Models of the Pulsatile Hydrodynamics of Cerebrospinal Fluid Flow in the Normal and Abnormal Intracranial System," Comput. Methods Biomech. Biomed. Engng. **10** (2), 151–157 (2007).
24. I. Sobey and B. Wirth, "Effect of Non-Linear Permeability in a Spherically Symmetric Model of Hydrocephalus," Math. Medicine Biology. **23** (4), 339–361 (2006).
25. J. Vardakis, L. Guo, T. Peach, et al., "Fluid-Structure Interaction for Highly Complex, Statistically Defined, Biological Media: Homogenisation and a 3D Multi-Compartmental Poroelastic Model for Brain Biomechanics," J. Fluids Structures **91**, 102641 (2019).
26. O. Coussy, *Poromechanics* (John Wiley and Sons, Chichester, 2004).
27. A. Smillie, I. Sobey, and Z. Molnar, "A Hydroelastic Model of Hydrocephalus," J. Fluid Mech. **539**, 417–443 (2005).
28. B. Tully and Y. Ventikos, "Coupling Poroelasticity and CFD for Cerebrospinal Fluid Hydrodynamics," IEEE Trans. Biomed. Engng. **56** (6), 1644–1651 (2009).
29. Z. Taylor and K. Miller, "Reassessment of Brain Elasticity for Analysis of Biomechanisms of Hydrocephalus," J. Biomech. **37** (8), 1263–1269 (2004).
30. F. Hecht, "New Development in FreeFem++," J. Numer. Math. **20**, 251–265 (2012).
31. I. Johnston and C. Teo, "Disorders of CSF Hydrodynamics," Child's Nervous System **16** (1011), 776–799 (2000).
32. C. E. Johanson, J. A. Duncan, P. M. Klinge, et al., "Multiplicity of Cerebrospinal Fluid Functions: New Challenges in Health and Disease," Cerebrospinal Fluid Res. **5** (1), 1–32 (2008).
33. G. S. Yan'kova, A. A. Cherevko, A. K. Khe, et al., "Study of Hydrocephalus Using Poroelastic Models," Prikl. Mekh. Tekh. Fiz. **61** (1), 17–29 (2020) [J. Appl. Mech. Tech. Phys. **61** (1), 14–24 (2020)].